Am J Cancer Res 2021;11(5):1982-2004
www.ajcr.us /ISSN:2156-6976/ajcr0126846

Original Article

βKlotho, a direct target of miR-206, contributes to the growth of hepatoblastoma through augmenting PI3K/Akt/mTOR signaling

Tong Chen*, Jianglong Chen*, Xiuhao Zhao, Jing Zhou, Qingfeng Sheng, Linlin Zhu, Zhibao Lv

*Department of General Surgery, Shanghai Children's Hospital, Shanghai Jiao Tong University, Shanghai 200040, P. R. China. *Equal contributors.*

Received November 23, 2020; Accepted March 10, 2021; Epub May 15, 2021; Published May 30, 2021

Abstract: Hepatoblastoma (HB) is the most frequent pediatric liver malignancy. However, the treatment outcome for patients with advanced-stage HB remains unsatisfactory. Accumulating evidence indicates that βKlotho (KLB) acts as an oncogene or a tumor-suppressor gene in a context-dependent manner. Despite this, the expression profile and effects of KLB on the growth of HB are still elusive. This study aimed to explore the effect of miR-206/KLB axis on HB growth. The expression of KLB was explored in HB cells (HepG2 and HuH6) and tissues using quantitative polymerase chain reaction (qPCR), Western blot analysis, and immunohistochemistry. Besides, miR-206 expression was determined in HB cells and tissues using qPCR and fluorescence in situ hybridization. The prognostic value of KLB or miR-206 in our patients with HB was investigated using the Kaplan-Meier method. The biological effects of KLB or miR-206 on HB cells were identified *in vitro*. The proliferative effects of KLB on HuH6 cells were also investigated *in vivo*. Moreover, the mechanical signaling of KLB in HB was determined through bioinformatics analysis followed by experimental validation. The results showed a significant upregulation of KLB in HB tissues and cells. Elevated level of KLB was found to be significantly correlated with the aggressive phenotype and poor overall survival for children with HB. The *in vitro* function assay demonstrated that KLB knockdown promoted apoptosis and suppressed the proliferation, migration, and invasion of HB cells. Besides, KLB knockdown inhibited the proliferation of HuH6 cells *in vivo*, while KLB overexpression had the opposite effect. Furthermore, KLB was proved to be the direct target of miR-206. Low level of miR-206 served as an independent risk factor for poor prognosis in children with HB. The overexpression of miR-206 negatively regulated the aggressive biological behaviors of HB cells, which was partially rescued by KLB overexpression. Mechanically, the miR-206/KLB axis played a vital role in HB growth through augmenting the phosphatidylinositol 3-kinase (PI3K)/Akt/mammalian target of rapamycin (mTOR) signaling. In conclusion, the data demonstrated that the miR-206/KLB axis might serve as an important biomarker/therapeutic target for HB.

Keywords: Akt, hepatoblastoma, KLB, miR-206, mTOR, PI3K

Introduction

Hepatoblastoma (HB) accounts for more than 80% of pediatric liver malignancy [1], and an increasing trend of its incidence has been reported in a number of countries [1, 2]. Nevertheless, HB is a relatively rare tumor, affecting approximately 1.8 cases per million children per year [3]. Although the combination of chemotherapy and surgery has improved the outcomes for pediatric patients with HB, the prognosis of advanced-stage HB remains poor, with a 3-year event-free survival as low as 34% [4]. Therefore, defining novel therapeutic strategies is urgently needed for treating advanced-stage HB.

The klotho family proteins, including Klotho (or αKlotho), βKlotho (KLB), and γklotho, play crucial roles in aging, muscle regeneration [5], and energy metabolism [6]. KLB shares 41% amino acid sequence homology with αKlotho [7]. It is a single-pass transmembrane protein critical for mediating transmembrane signaling [8]. Recent years have witnessed extensive research on the effect of KLB on the initiation and progression of various human tumors. Specifically, KLB was identified as a tumor sup-

Table 1. GEO information used in this study

GEO ID	Platforms	Non-tumor	Tumor	Year	Country
GSE131329	Affymetrix mRNA microarray	14	53	2019	Japan
GSE75271	Affymetrix mRNA microarray	5	50	2016	USA
GSE75283	Agilent miRNA microarray	8	57	2017	USA

pressor in prostate cancer [9], endometrial carcinoma [10], and lung cancer [11]. On the contrary, KLB promoted the growth of bladder cancer [12] and had oncogenic activities in hepatocellular carcinoma (HCC) [13, 14]. Yet, paradoxically, KLB was also demonstrated to inhibit the growth of HCC in association with fibroblast growth factor receptor 4 (FGFR4) [15]. Furthermore, the downregulation of KLB was found in liver tissues in children with non-alcoholic fatty liver disease [16] and adults with hepatic fibrosis [17]. Collectively, KLB acts as either an oncogene or a tumor-suppressor gene in a highly context-dependent manner, yet the effect of KLB on HB still remains unclear.

MicroRNAs (miRNAs) are small single-stranded RNA molecules of ~22 nucleotides in length that negatively regulate gene expression [18]. A sizable evidence base demonstrates the important effects of miRNAs on the initiation and progression of human tumors, such as HB. Specifically, a variety of miRNAs have been suggested to be implicated in the initiation and progression of HB, including miR-17, miR-21, miR-124, miR-492, and miR-34a-5p [19-21]. Further, miR-206 was reported to play a tumor-suppressive role in a number of human tumors, including head and neck squamous cell carcinoma (HNSCC), HCC, colonic tumors, and osteosarcoma [22-25]. However, the specific effect of miR-206 on HB growth still remains undetermined. Additionally, whether miR-206 can alter tumorigenesis by targeting KLB has never been experimentally reported to date.

This study showed the upregulation of KLB in both HB tissues and cells. The *in vitro* experiment showed that the knockdown of KLB induced apoptosis and suppressed the proliferative, migratory, and invasive capacities of HB cells. Furthermore, KLB knockdown suppressed the proliferation of HB cells, whereas an opposite effect was detected for KLB overexpression. Moreover, miR-206 directly targeted KLB by binding to its 3'-untranslated region (3'-UTR). The overexpression of miR-206 suppressed the proliferative, migratory and invasive capacities of HB cells, which could be partially rescued by KLB overexpression. Clinically, both KLB upregulation and miR-206 downregulation served as independent adverse prognostic factors in pediatric patients with HB. Mechanically, the miR-206/KLB axis played a vital role in regulating the phosphatidylinositol 3-kinase (PI3K)/Akt/mammalian target of rapamycin (mTOR) pathway. Overall, the data demonstrated that miR-206/KLB acted as a novel regulatory axis for HB, which might be a promising target for therapeutic strategies in HB.

Materials and methods

Datasets

Three independent microarrays, namely, GSE131329, GSE75271, and GSE75283 datasets, were accessed from Gene Expression Omnibus (GEO) to explore KLB or miR-206 expression in HB or non-tumor liver tissues. **Table 1** illustrates the specific features of these three microarrays. Besides, bioinformatics resources, including Gene Set Variation Analysis (GSVA) and Kyoto Encyclopedia of Genes and Genomes (KEGG), were also used.

Human HB samples

Between January 2010 and December 2019, paraffin-embedded HB tissues and matched normal liver tissues were taken from 48 children who had undergone surgical excision for primary HB at the hospital. Besides, immediately after surgical resection, HB and matched non-tumor liver tissues from eight children were snap-frozen in liquid nitrogen, and then kept at -80°C. The pathological diagnosis of each patient was confirmed by a panel of expert pathologists blind to patient clinical information. The follow-up of these 48 patients was performed routinely at the hospital. The institutional ethics committee at the hospital approved the study, and the parents or legal

guardians of these pediatric patients gave written informed consent.

Cell lines and culture

Human HB cell lines (HepG2 and Huh6), human liver cells (LO2 and Chang Liver), and embryonic kidney cells (HEK-293T) were obtained from the Chinese Academy of Sciences (Shanghai, China). The cells were seeded in Dulbecco modified Eagle medium (DMEM) containing 10% fetal bovine serum (FBS) at 37°C with 5% CO_2.

Reagents and antibodies

FBS (Cat. no. 10099141), DMEM (Cat. no. 11995065), 0.25% Trypsin-EDTA (Cat. no. 25200072), penicillin/streptomycin (Cat. no. 15140122), and PBS (Cat. no. 10010023) were procured from Gibco (NY, USA). The antibodies against KLB (Cat. no. ab106794), Akt (Cat. no. ab8805), PI3K (Cat. no. ab191606), p-PI3K (Cat. no. ab182651), caspase 3 (Cat. no. ab13847), and Ki67 (Cat. no. ab15580) were purchased from Abcam (MA, USA). The antibodies against mTOR (Cat. no. 2972S), p-mTOR (Cat. no. 2971S), and GAPDH (Cat. no. 5174S) were obtained from CST (MA, USA), while the antibody against p-Akt (Cat. no. 66444-1-Ig), and GAPDH (Cat no. 10494-1-AP) were purchased from Proteintech (IL, USA).

Quantitative polymerase chain reaction

TRIzol (Life Technologies, CA, USA) was used to isolate total cellular RNAs. Reverse transcription was conducted using TaKaRa reverse transcription kit (TaKaRa Bio, Shiga, Japan) except for miR-206. Regarding miR-206, the first-strand cDNA was synthesized using a stem-loop method reverse transcription kit (Sangon, Shanghai, China). The SYBR Green fluorescence system (Roche, IN, USA) was used. Moreover, quantitative polymerase chain reaction (qPCR) of mRNAs was conducted using a quantitative mRNA kit (TaKaRa Bio), whereas qPCR of miRNAs was carried out with an miRNA qPCR kit (Sangon). Levels of mRNA and miRNA were normalized relative to GAPDH mRNA and U6 miRNA, respectively. The relative level of mRNA or miRNA was computed based on the $2^{-\Delta\Delta Ct}$ method. The primers (synthesized in Sangon) used were as follows: KLB: 5'-AGGTACTACAGGTGCGTGGTCAG-3' (sense), 5'-CGGTTAGGCTCGTTGATGGTGATC-3' (antisense); GAPDH: 5'-GGCACCGTCAAGGCTGAGAAC-3' (sense), 5'-GGTGGCAGTGATGGCATGGAC-3' (antisense); miR-206: 5'-GGAATGTAAGGAAGTGTG-3' (sense), 5'-GAGCAGGCTGGAGAA-3' (antisense); U6: 5'-CTCGCTTCGGCAGCACA-3' (sense), 5'-AACGCTTCACGAATTTGCGT-3' (antisense).

Western blot analyses

The cells or tissues were lysed using radioimmunoprecipitation assay (RIPA) buffer supplemented with cocktail and PMSF. The lysates were separated using SDS-PAGE, followed by transfer onto the PVDF membrane. Next, the membrane was incubated with blocking buffer for 1 h. The membrane was incubated with a primary antibody, followed by incubation with an IgG HRP-conjugated secondary antibody (Jackson ImmunoResearch, PA, USA) for 2 h. The protein detection was achieved using the ChemiDoc-It system (Tanon, Shanghai, China). The band intensities were determined using ImageJ software. GAPDH served as a loading control.

Immunohistochemistry

Human HB samples were fixed with paraformaldehyde (PFA) and paraffin-embedded. Sections of 5 um were prepared and mounted on slides. Then, the sections were deparaffinized and rehydrated, followed by antigen retrieval. Subsequently, the tissue sections were incubated with a primary antibody in a humidified chamber under 4°C overnight, followed by incubation with an HRP-coupled secondary antibody. The immunohistochemistry (IHC) scores comprised two components: the frequency of immune-positive cells and staining intensity [26]. The frequency was graded as 0 for no immune-positive cells, 1 for 1%-10% immune-positive cells, 2 for 11%-50% immune-positive cells, 3 for 51%-80% immune-positive cells, and 4 for 81%-100% immune-positive cells. The staining intensity was defined as 0 for negative, 1 for weak, 2 for moderate, and 3 for strong. Subsequent IHC scores were calculated by multiplying these two scores. Therefore, the minimal IHC score could be as low as 0, and the maximum score might be as high as 12. Further, the IHC score of more than 6 was regarded as a typical "high" value, whereas the IHC score of less than 6 was thought to be a typical "low" value. The IHC scores were evaluated blindly by two independent pathologists.

Fluorescence in situ hybridization

Paraformaldehyde-fixed human HB sample were paraffin-embedded and sectioned. Fluorescence *in situ* hybridization (FISH) was performed using a miR-206 Probe Kit (RiboBio, Guangzhou, China) following the manufacturer's protocols. The sequence of miR-206 probe was 5'-CY3-CCACACACUUCCUUACAUUCCA-3'. The fluorescence intensity of each spot was estimated with an epifluorescence microscope (Olympus, Tokyo, Japan). The fluorescence intensities of miR-206 dyeing were classified into four staining grades: 1+, weak; 2+, intermediate; 3+, strong; 4+, very strong. Further, the staining grades were categorized into the following two groups: low (score 1+ or 2+) and high (score 3+ or 4+).

Immunofluorescence

The cells were cultured in 12-well plates. After reaching 50% confluence, the cells were washed with PBS three times, fixed in PFA for half an hour, and then soaked in absolute ethyl alcohol for 20 min. After incubation with blocking buffer for half an hour, the cells were stained with primary antibodies overnight at 4°C. After washing nonspecific binding antibodies, secondary antibodies (Jackson Immuno Research) were added with the exclusion of light for 1 h at room temperature. Subsequently, the cell nuclei were viewed using the mounting solution with 4',6-Diamidino-2-phenylindole (DAPI) (Sigma, MO, USA) for 5 min at room temperature and then washed with PBS three times. Finally, the stained cells were viewed using a microscope.

Plasmids and small interfering RNA

KLB small interfering RNA (siRNA)/plasmid, miR-206 mimic/inhibitor, or non-targeting NC (GenePharma, Shanghai, China) was transfected into cells using Lipofectamine 2000 following the manufacturer's protocols. The efficiencies of siRNAs were established using qPCR and Western blot (WB) 48-72 h after transfection. The sequences of different siRNAs were listed as follows: KLB siRNA: 5'-GCAAUAAGGUUAGAUGAAAUACGAG-3'; Control siRNA: 5'-UUCUCC GAACGUGUCACGUTT-3'; miR-206 mimic: 5'-UGGAAUGUAAGGAAGUGUGUGG-3'; miR-206 inhibitor: 5'-CCACACACUUCCUUACAUUCCA-3'; miR-206 mimic NC: 5'-CCACACAUUCCUUACAUUCCA-3'; miR-206 inhibitor NC: 5'-CAGUACUUUUGUGUAGUACAA-3'.

Luciferase assay

The plasmids, including pmirGLO-KLB 3'-UTR (634 bp-WT, H16675) and pmirGLO-KLB 3'-UTR (634 bp-MUT, H16676), were constructed using Obio Technology (Shanghai, China). HEK-293T cells were co-transfected with H16675 plus NC, H16675 plus miR-206 mimic, H16676 plus NC, or H16676 plus miR-206 mimic with Lipofectamine 2000 (Invitrogen Co., CA, USA) following the manufacturer's protocols. After 2 days, the luciferase activity was evaluated using a Dual Luciferase Assay System (Promega, WI, USA).

Wound-healing assay

The wells from six-well plates were seeded with an HepG2 or HuH-6 cell line at a density of 5×10^6 cells/well. After reaching 90% confluence, the model wound was created using a sterilized pipette tip. The wounded areas were photographed under the microscope every 24 h, and the migration distances were quantified. Representative images were taken at × 40 magnification.

Cell viability assay

The viability of cells was assessed using a cell counting kit-8 (CCK8, Dojindo, Japan). The cells were seeded in a 96-well plate (at a density of 1×10^3 cells per well) and kept for 4 h until cell adherence. Later, CCK8 reagent was added to each well at the indicated time point. After 1 h, the plate was read at 450 nm to determine optical density.

Colony formation assay

The cells at a density of 3×10^3 cells/well were seeded in six-well plates in a medium containing 10% FBS. The next day, the culture media were replaced by the media with 5% FBS and then cultured for 12 days. Then, the cells were PFA-fixed and stained with crystal violet. Later, the images were taken.

Transwell assay

The Transwell assays were conducted using 24-well plates with Transwell inserts (8-um pore size; BD Biosciences, USA) following the

manufacturer's protocols. Regarding the migration assay, the cells were seeded into the upper chambers with serum-free DMEM. The lower chambers were complemented with 10% FBS. After 24 h, the cells on the top of membranes were removed. For invasion assays, Matrigel obtained from BD Biosciences was placed in the media without serum, transferred into the top chamber, and incubated for 5 h. Subsequently, the cells were seeded into top chambers containing the media without serum. On the contrary, the bottom chambers were supplemented with 10% FBS. After 36 h, the cells on the top chamber were removed. For quantification, the membranes were PFA-fixed and stained with crystal violet. Later, the migrated/invaded cells were observed, photographed and counted.

Tumor xenografts

HuH6 cells were stably transfected with KLB knockdown lentivirus (KLB-KD), KLB overexpression lentivirus (KLB-OE), and NC lentivirus (KLB-EV) from GeneChem (Shanghai, China). To achieve HuH6 cell line xenograft tumors, 10^7 HuH6 cells were engrafted with 100 μL of Matrigel in 5- to 6-week-old male BALB/c nude mice subcutaneously. Each experimental group comprised five mice, and each mouse was cultured under specific pathogen-free conditions. The mice were evaluated every 3 days for body weight and tumor size. The tumor volumes were computed using the formula: length × $(\text{width})^2$ × π/6. After 4 weeks, the xenografts were harvested and preserved for further analysis. All mice were maintained in accordance with the National Institutes of Health (NIH) animal care guidelines, and the animal experiment committee at the hospital approved all mouse experiments.

Statistical analysis

SPSS 22.0 (IBM, New York, USA) and GraphPad Prism v7.0 (GraphPad, CA, USA) were used for statistical analysis. Bivariate analyses were performed using the two-tailed χ^2 test or Fisher's exact test for categorical variables and the Student *t* test for continuous variables. The overall survival of pediatric patients with HB was evaluated using the Kaplan-Meier method and log-rank test. Univariate and multivariate Cox models were used to explore the influence of different variables on the prognosis. The correlation was evaluated using the Spearman rank correlation method. A *P* value of less than 0.05 indicated a statistically significant difference.

Results

Overexpression of KLB in HB tissues and cells

qPCR and WB analyses were conducted on HB and matched non-tumor liver tissues from eight children to determine the expression pattern of KLB in HB and normal liver tissues. The qPCR data revealed elevated KLB levels in HB tissues compared with control tissues (**Figure 1A**), which was further validated via WB analysis (**Figure 1B**). Also, KLB protein expression levels in HB samples from 48 patients were determined by IHC. Consistent with the former result, KLB expression levels were significantly elevated in HB tissues compared with adjacent normal liver tissues. Additionally, the representative staining pattern of HB/normal tissues was presented (**Figure 1C**). Further, KLB expression in HB cell lines (HepG2 and HuH6) and normal liver cell lines (L02 and Chang Liver) was explored. WB data revealed significantly elevated expression of KLB in HB cell lines compared with normal liver cell lines (**Figure 1D**).

KLB expression correlated with poor prognosis in children with HB

The χ^2 tests and Fisher exact tests were used to explore the correlations of KLB levels with the clinicopathological variables. The elevated KLB levels had a correlation with distant metastasis, recurrence, and higher COG stage (**Figure 2A-C** and **Table 2**). Kaplan-Meier analysis indicated that the prognosis of children with HB having higher KLB expression was markedly poorer compared with the prognosis of those with lower KLB expression (**Figure 2D**). In addition, univariate and multivariate Cox models identified distant metastasis, recurrence, higher COG stage, and elevated KLB level as independent adverse prognostic factors for patients with HB (**Figure 2E** and **Table 3**).

KLB knockdown suppressed HB proliferation in vitro and in vivo

KLB knockdown was achieved in both HepG2 and HuH6 cell lines using KLB-siRNA to investi-

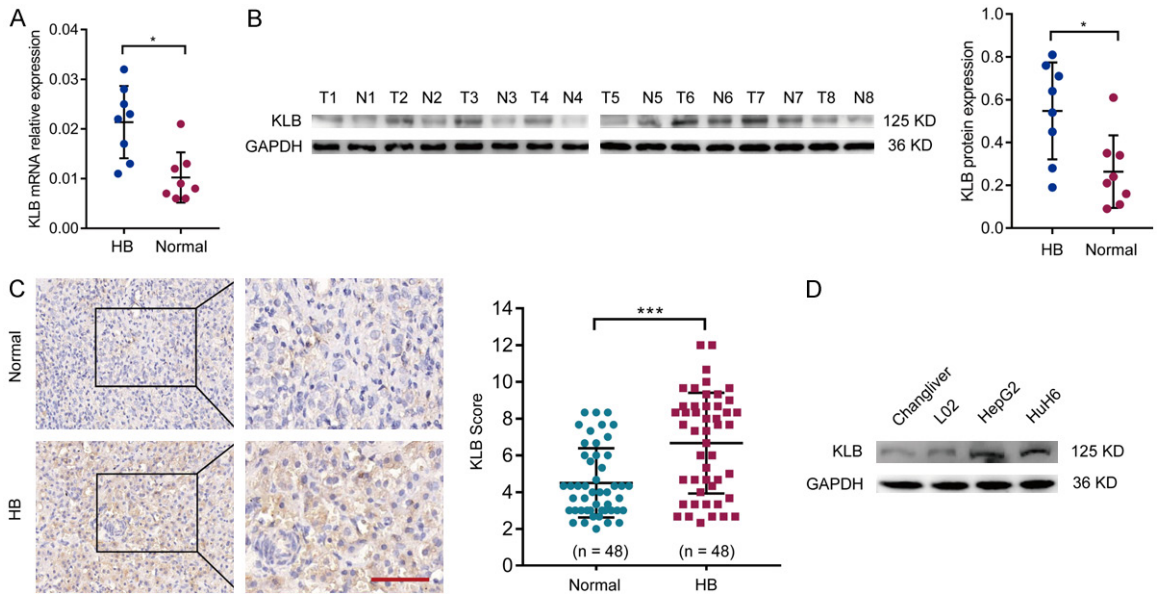

Figure 1. Upregulation of KLB in HB tissues and cells. A. KLB mRNA level (normalized to GPADH level) was explored by qPCR in HB tissues compared with their adjacent normal tissues. B. WB analysis revealed KLB expression of HB and adjacent normal liver tissues in eight patients. Relative quantification of KLB protein levels, normalized to GAPDH levels, was also determined. C. Representative IHC KLB staining in HB and matched normal liver tissues. The IHC scores of KLB were compared between HB tissues (n = 48) and matched non-tumor liver tissues (n = 48). Scale bars, 100 μm. D. WB analysis revealed KLB expression in different cell lines. HB, Hepatoblastoma; IHC, immunohistochemistry; WB, Western blot. *$P < 0.05$. Original WB images are presented in Figure S1.

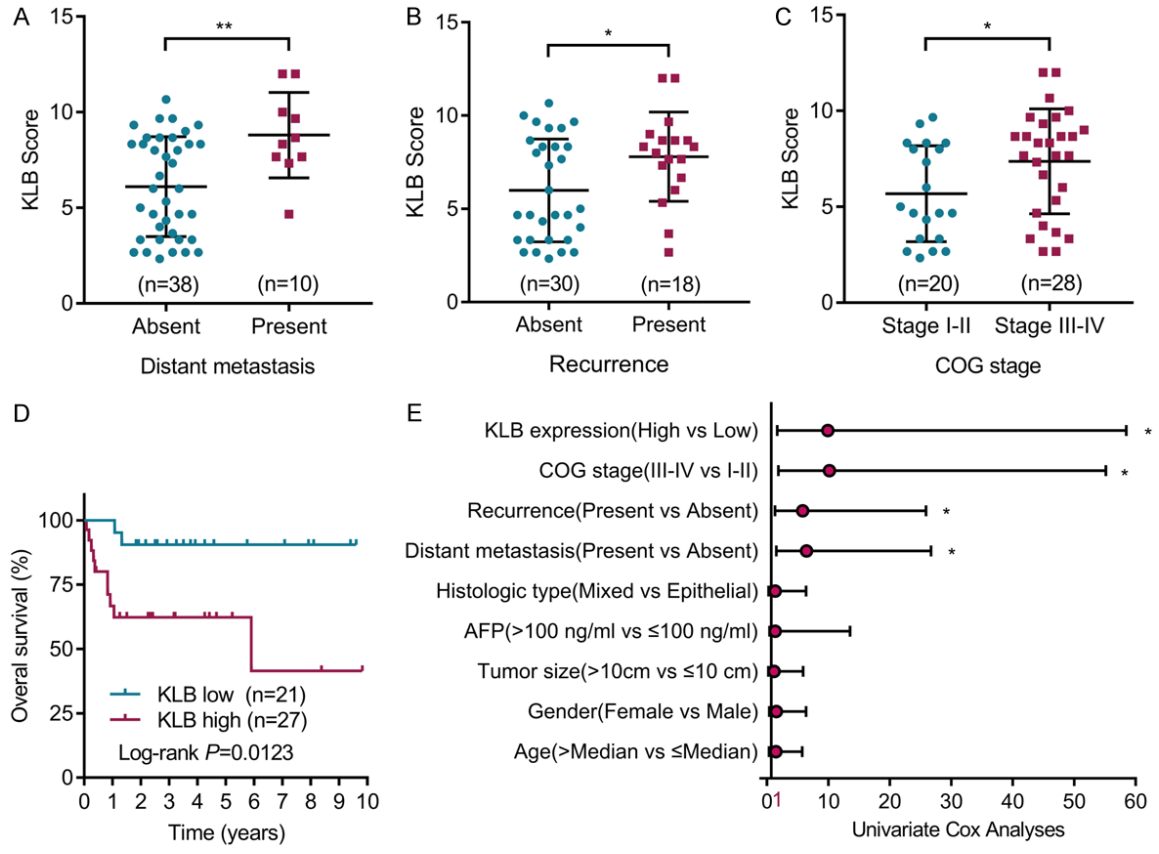

Figure 2. Elevated levels of KLB correlated with poor overall survival for pediatric patients with HB. Expression levels of KLB in patients with HB from the hospital in the presence or absence of (A) distant metastasis or (B) recurrence. (C) Expression levels of KLB in patients with HB having low or high COG stage. (D) Kaplan-Meier method revealed the association between KLB expression and prognosis in children with HB from the hospital. (E) Univariate Cox regression analysis disclosed correlations between different clinicopathological variables and KLB expression. *P < 0.05, **P < 0.01.

Table 2. Correlation among KLB, miR-206 levels, and clinicopathological features

Clinicopathological features		No. of cases	KLB		P value	miR-206		P value
			Low (n = 21)	High (n = 27)		Low (n = 24)	High (n = 24)	
Age (years)	≤ Median	24	9	15	0.383	12	12	1.000
	> Median	24	12	12		12	12	
Gender	Male	23	8	15	0.230	14	9	0.248
	Female	25	13	12		10	15	
Tumor size	≤ 10 cm	29	15	14	0.169	9	20	0.003
	> 10 cm	19	6	13		15	4	
AFP	≤ 100 ng/ml	43	18	25	0.641	22	21	0.637
	> 100 ng/ml	5	3	2		2	3	
Histologic type	Epithelial	18	8	10	0.940	9	9	1.000
	Mixed	30	13	17		15	15	
Metastasis	Absent	38	20	18	0.029	15	23	0.005
	Present	10	1	9		9	1	
Recurrence	Absent	30	17	13	0.034	7	23	< 0.001
	Present	18	4	14		17	1	
COG stage	Stage I-II	20	14	6	0.002	4	16	< 0.001
	Stage III-IV	28	7	21		20	8	

gate the effect of KLB expression on HB cells. The knockdown efficiency of KLB by siRNA at different concentrations was confirmed by WB analysis (**Figure 3A**). After transfection of KLB-siRNA into HepG2 and HuH6 cells, the effects of KLB knockdown on cell proliferation were determined through the immunofluorescence (IF) staining of Ki67 (**Figure 3B**). The percentages of Ki67 positive cells were significantly lower among KLB-siRNA cells compared with control cells. In addition, CCK-8 assays (**Figure 3C**) and colony formation assays (**Figure 3D**) indicated significantly lower proliferation capacities in the KLB-siRNA group compared with the control group.

Next, the roles of KLB expression in HB cells were also investigated in vivo. HuH6 cells were stably transfected with KLB-KD, KLB-KD-NC, KLB-OE, or KLB-OE-NC lentivirus vectors. The KLB-KD group exhibited a significant reduction in tumor volume (**Figure 3E** and **3F**). Contrarily, a significant increase in tumor volume was observed in the KLB-OE group compared with the control group (**Figure 3E** and **3F**). Despite no significant differences in body weight among different groups (**Figure 3G**), the KLB-KD group had a significantly decreased tumor volume (**Figure 3H**), and significantly decreased Ki67 expression in tumor tissues (**Figure 3I**) compared with the control group. Meanwhile, the KLB-OE group had a significantly elevated tumor volume compared with the control group. Collectively, the results demonstrated that KLB knockdown suppressed the proliferative abilities of HB cell lines *in vitro* and *in vivo*, whereas KLB overexpression promoted the proliferative abilities of HB cell lines *in vivo*.

KLB knockdown promoted apoptosis and inhibited the migration and invasion of HB cells

After transfection of KLB-siRNA into HepG2 and HuH6 cell lines, IF staining of caspase 3 indicated that the KLB-siRNA group had a significantly elevated percentage of caspase 3 immuno-positive cells compared with the control group (**Figure 4A**). Subsequently, the effects of KLB knockdown on cell migration were assessed using the wound-healing assay

Table 3. Univariate and multivariate analyses of prognosis for patients with HB

Clinicopathological features		Univariate analyses		*P* value	Multivariate analyses		*P* value
		HR	95% CI		HR	95% CI	
Age (years)	≤ Median	1.436	0.359-5.740	0.609			
	> Median						
Gender	Male	1.541	0.374-6.344	0.550			
	Female						
Tumor size	≤ 10 cm	1.152	0.226-5.869	0.865			
	> 10 cm						
AFP	≤ 100 ng/ml	1.328	0.430-13.536	0.358			
	> 100 ng/ml						
Histologic type	Epithelial	1.336	0.281-6.355	0.716			
	Mixed						
Metastasis	Absent	6.419	1.543-26.700	0.011	1.000		
	Present				6.295	2.018-19.636	0.002
Recurrence	Absent	5.821	1.309-25.892	0.021	1.000		
	Present				4.274	1.321-13.826	0.015
COG stage	Stage I-II	10.150	1.869-55.131	0.007	1.000		
	Stage III-IV				8.367	1.682-41.619	0.009
KLB	Low	9.916	1.682-58.457	0.011	1.000		
	High				9.555	1.912-47.765	0.006

(**Figure 4B**). The relative migration distance of HB cells was markedly lower in the KLB-siRNA group compared with the control group. Consistently, Transwell migration assays also suggested that the KLB-siRNA group had a significantly lower rate of relatively migrating cells compared with the control group (**Figure 4C**). In addition, these assays revealed a markedly decreased rate of relatively invading cells in the KLB-siRNA group compared with the control group (**Figure 4D**). Overall, KLB knockdown promoted apoptosis and suppressed the migratory and invasive capabilities of HB cells.

KLB served as the direct target gene of miR-206 in HB

A total of 12 databases (Targetscan, Microt4, miRMap, miRcode, miRanda, mirbridge, miRDB, PITA, miRNAMap, Pictar2, RNA22, and RNAhybrid) were used to screen the predicted miRNAs targeting KLB. Three miRNAs, including miR-206, miR-1, and miR-193a-3p, were predicted to target KLB in eight databases; all the other miRNAs were predicted to target KLB in fewer than eight databases. Subsequently, using one publicly available microarray dataset (GSE75283), the expression levels of both miR-206 and miR-193a-3p were found to be significantly lower in HB samples compared with normal liver samples; however, it was not the case for miR-1 ($P = 0.1654$). A literature search revealed miR-193a-3p as a previously reported tumor-suppressive miRNA in HB [27]; the role of miR-206 in HB growth has not been reported to date. Therefore, miR-206 was selected for subsequent experimental validation. The predicted target site of KLB 3'UTR for miR-206 is shown in **Figure 5A**. Further, qPCR and WB analyses showed that miR-206 expression had an inverse correlation with KLB expression in HB cells. The upregulation of miR-206 markedly suppressed KLB expression, whereas KLB expression was promoted after miR-206 suppression (**Figure 5B** and **5C**). Subsequently, the relative luciferase activities of HEK-293T cells after co-transfection with WT-KLB and miR-206 mimic significantly decreased compared with those in HEK-293T cells after co-transfection with Mut-KLB plus miR-206 mimic, establishing a direct relationship between miR-206 and 3'-UTR of KLB mRNA (**Figure 5D**). Moreover, miRNA microarray analysis confirmed markedly lower levels of miR-206 in tumor tissues compared with adjacent liver tissues (**Figure 5E**). Later, FISH was performed in HB and paired adjacent normal liver tissues to determine miR-206 expression. The scores of miR-206 dyeing were categorized into four grades ranging from 1 to 4+. Based on this, scores of 1+ and 2+ indi-

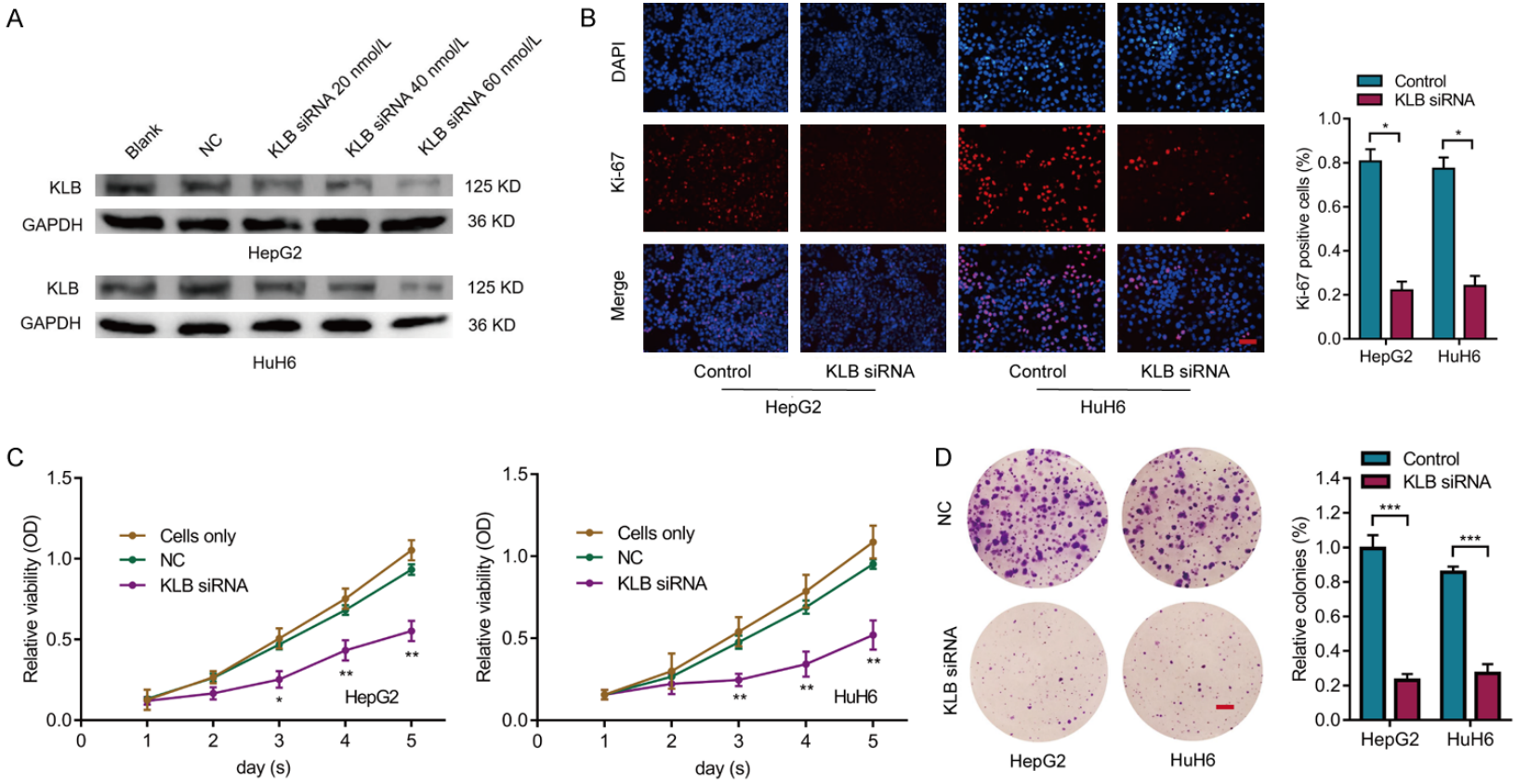
A
Blank
NC
KLB siRNA 20 nmol/L
KLB siRNA 40 nmol/L
KLB siRNA 60 nmol/L
KLB
GAPDH
125 KD
36 KD
HepG2
KLB
GAPDH
125 KD
36 KD
HuH6
B
DAPI
Ki-67
Merge
Control
KLB siRNA
Control
KLB siRNA
HepG2
HuH6
Control
KLB siRNA
Ki-67 positive cells (%)
HepG2
HuH6
C
Relative viability (OD)
Cells only
NC
KLB siRNA
HepG2
day (s)
Relative viability (OD)
Cells only
NC
KLB siRNA
HuH6
day (s)
D
NC
KLB siRNA
HepG2
HuH6
Control
KLB siRNA
Relative colonies (%)
HepG2
HuH6

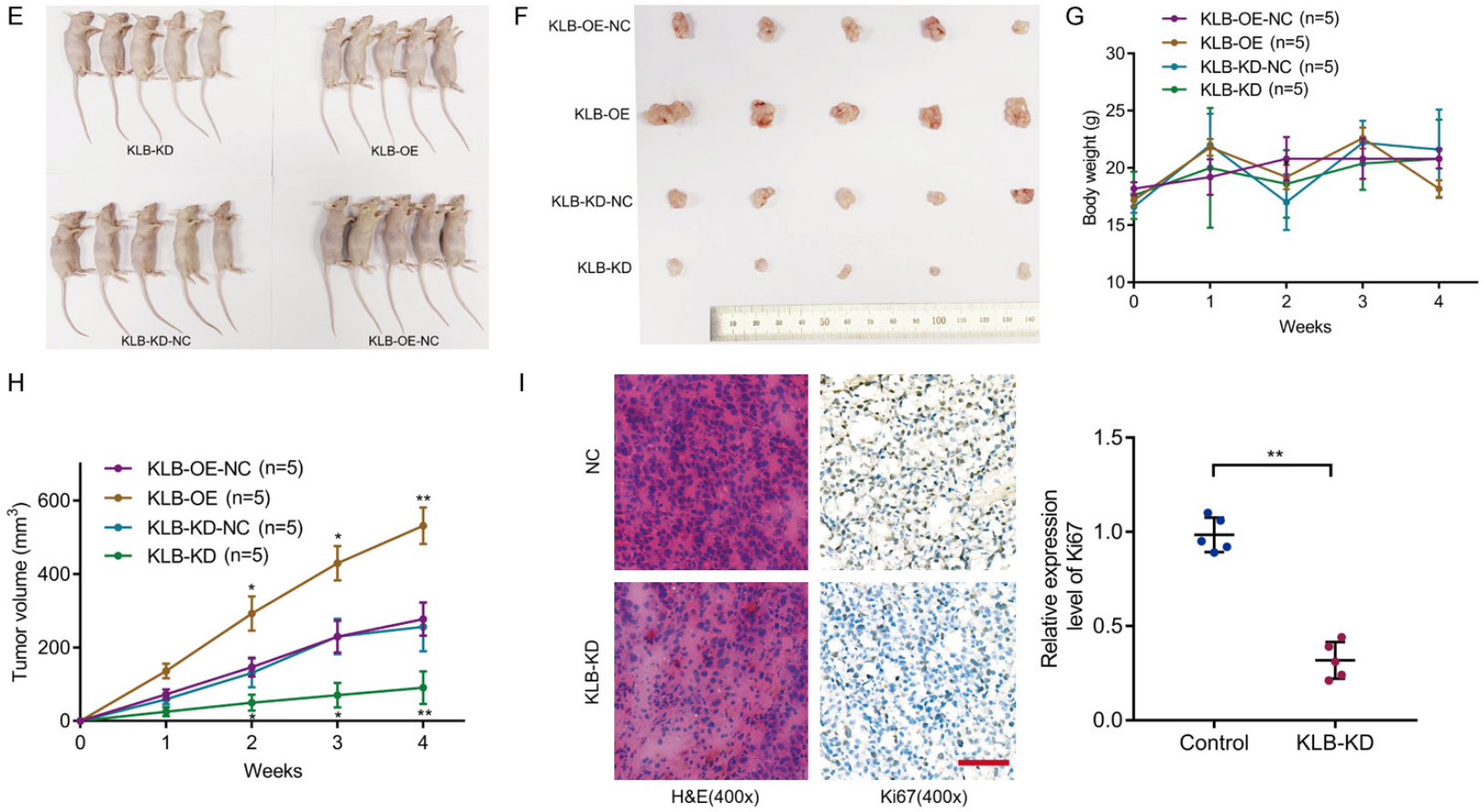

Figure 3. KLB knockdown suppressed the proliferation of HB cell lines in vitro and in vivo. (A) WB analysis revealed KLB knockdown efficiency after 48 h of transfection with siRNA. (B) After treatment with KLB or control siRNA, Ki67 was stained in red color; DAPI nuclear staining was in blue color. Scale bars, 100 μm. (C) CCK-8 assays displaying the proliferative capacity of HB cells after treatment with siRNA. (D) Colony formation assays showing the growth of HB cell lines after transfection with siRNA. Scale bars, 8 mm. (E) Photographs of nude mice xenografted subcutaneously with HuH6 cells among four groups. (F) Photographs of the tumors extracted from nude mice. (G) Body weight curve and (H) tumor growth curve were established. (I) IHC staining of Ki67 in tumors extracted from nude mice. Scale bars, 100 μm. CCK-8, Cell Counting Kit-8; HB, Hepatoblastoma; IF, immunofluorescence; IHC, immunohistochemistry; WB, Western blot. $*P < 0.05$, $**P < 0.01$, $***P < 0.001$. Original WB images are presented in Figure S1.

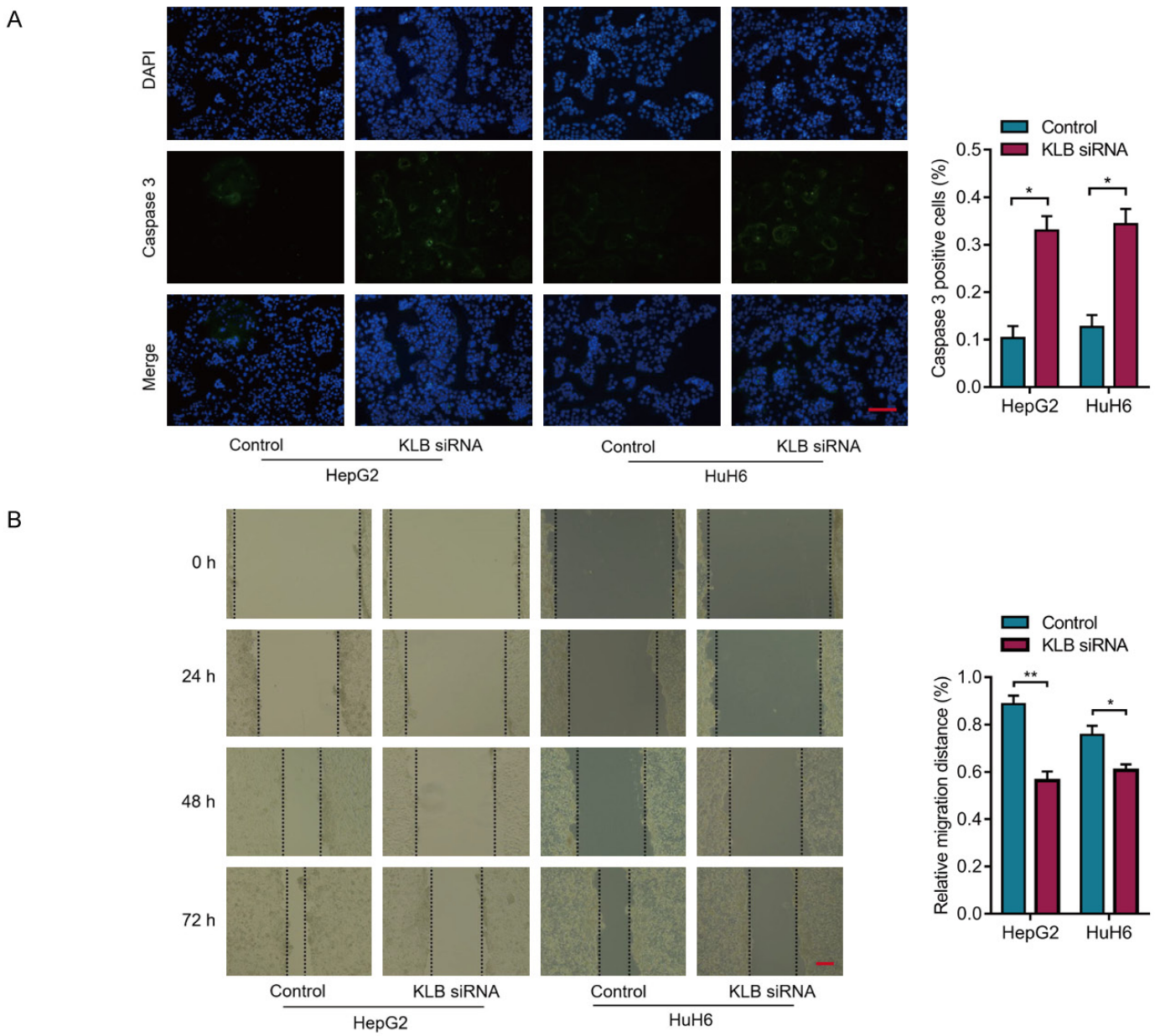
A
DAPI
Caspase 3
Merge
Control
KLB siRNA
HepG2
Control
KLB siRNA
HuH6
Control
KLB siRNA
Caspase 3 positive cells (%)
0.5
0.4
0.3
0.2
0.1
0.0
*
*
HepG2
HuH6
B
0 h
24 h
48 h
72 h
Control
KLB siRNA
HepG2
Control
KLB siRNA
HuH6
Control
KLB siRNA
Relative migration distance (%)
1.0
0.8
0.6
0.4
0.2
0.0
**
*
HepG2
HuH6

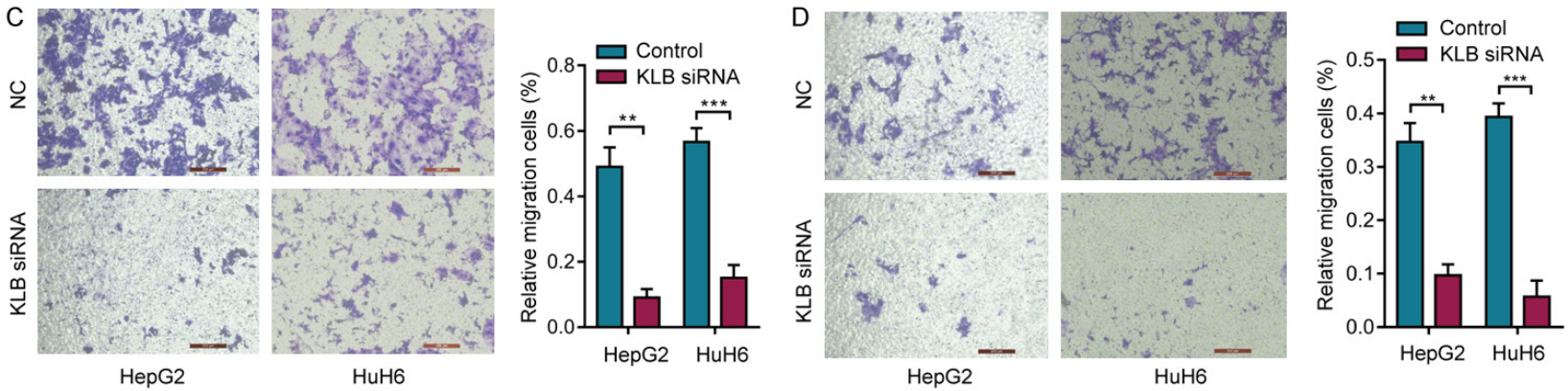

Figure 4. KLB knockdown promoted apoptosis and suppressed the migratory and invasive capacities of HB cells. (A) IF staining of caspase 3 (green) and DAPI (blue) in HB cell lines after transfection with siRNA. Scale bars, 100 μm. (B) Wound-healing assays showing the migration ability of HB cell lines after transfection. Scale bars, 500 μm. Transwell assays (scale bars, 200 μm) revealed (C) the migration capacity or (D) invasion capacity of HB cell lines after transfection. HB, Hepatoblastoma; IF, immunofluorescence. $*P < 0.05$, $**P < 0.01$, $***P < 0.001$.

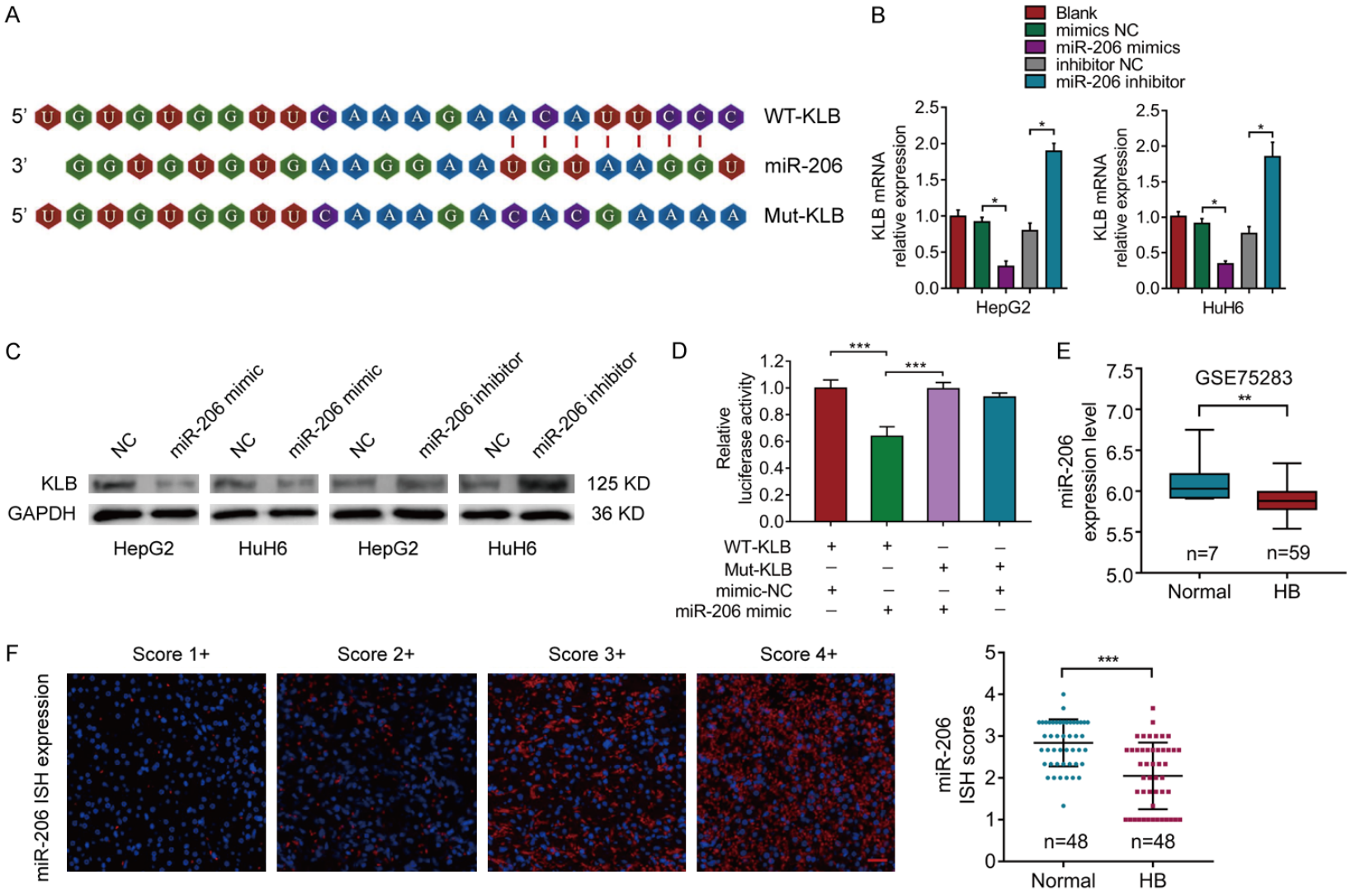
A
5'
3'
5'
WT-KLB
miR-206
Mut-KLB
B
Blank
mimics NC
miR-206 mimics
inhibitor NC
miR-206 inhibitor
KLB mRNA relative expression
HepG2
HuH6
C
NC
miR-206 mimic
miR-206 inhibitor
KLB
GAPDH
125 KD
36 KD
HepG2
HuH6
D
Relative luciferase activity
WT-KLB
Mut-KLB
mimic-NC
miR-206 mimic
E
GSE75283
miR-206 expression level
n=7
n=59
Normal
HB
F
Score 1+
Score 2+
Score 3+
Score 4+
miR-206 ISH expression
miR-206 ISH scores
n=48
n=48
Normal
HB

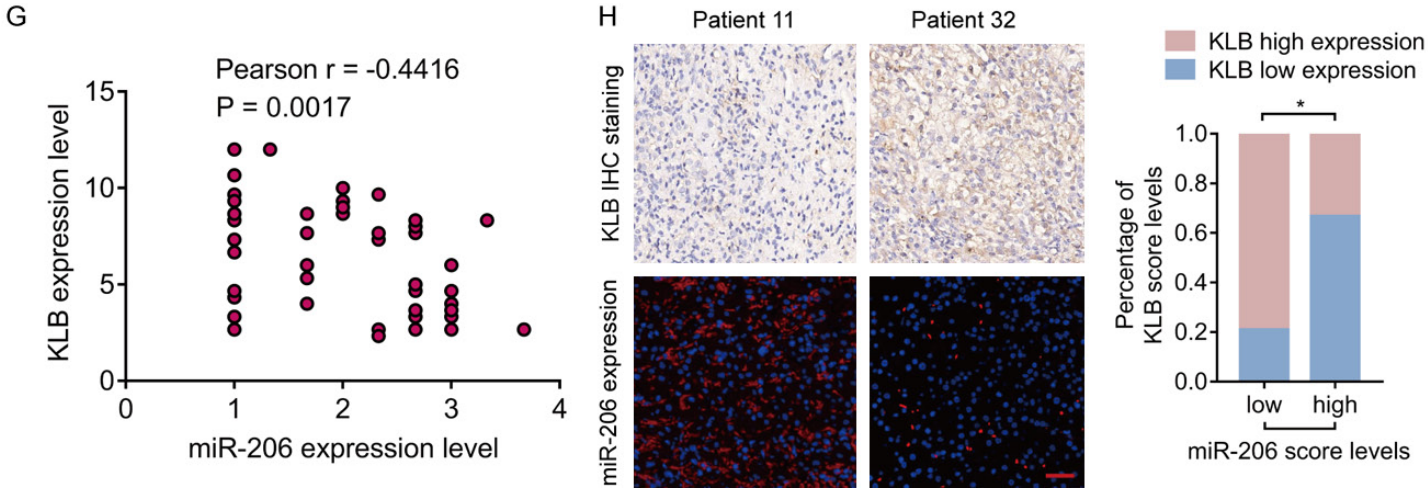

Figure 5. KLB served as a direct target of miR-206. A. Predicted binding sequences of miR-206, normal 3'-UTR of KLB, and mutated 3'-UTR of KLB. B. KLB mRNA expression (normalized to GAPDH) was established through qPCR in HB cell lines treated with miR-206 mimic, miR-206 inhibitor, or NC. C. WB analysis revealed KLB expression in HB cell lines transfected with miR-206 mimic, miR-206 inhibitor, or NC. D. Relative luciferase activities in the KLB-miR-206-wt and KLB-miR-206-mut groups. E. MiR-206 expression of HB and normal liver tissues based on the GSE75283 dataset. F. Representative miR-206 staining with different FISH grades of HB tissues. FISH scores for miR-206 in HB and adjacent non-tumor tissues were also determined. Scale bars, 100 μm. G. Pearson correlation analysis in patients showing the correlation between KLB expression and miR-206 expression in HB tissues. H. Representative staining (scale bars, 100 μm) for KLB and miR-206 of HB tissues in patients. Percentages of KLB staining grades with low or high miR-206 expression were also established. FISH, Fluorescence *in situ* hybridization; GEO, Gene Expression Omnibus database; HB, Hepatoblastoma; NC, negative control. $*P < 0.05$, $**P < 0.01$, $***P < 0.001$. Original WB images are presented in Figure S1.

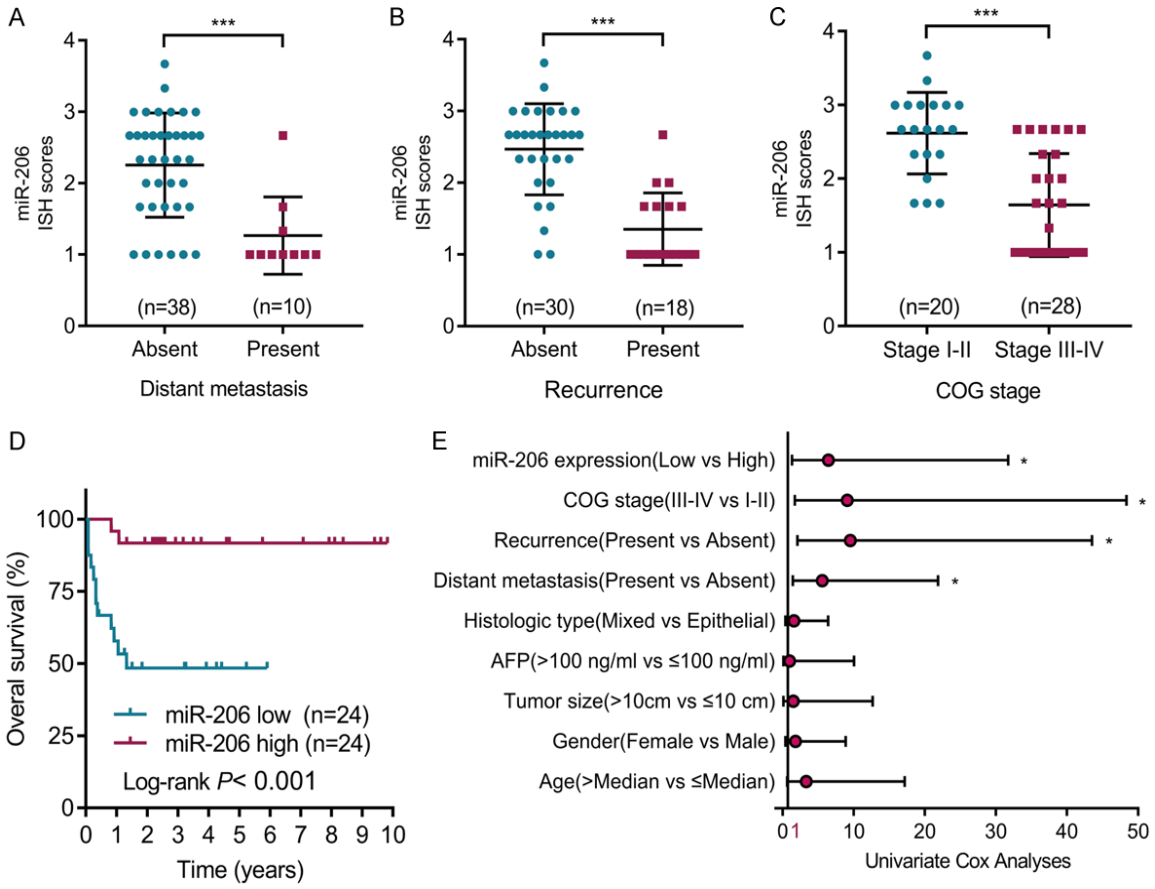

Figure 6. Expression of miR-206 correlated with poor prognosis in children with HB. The comparison of miR-206 staining scores between patients with HB in the absence or presence of (A) distant metastasis or (B) recurrence. (C) Comparison of miR-206 staining scores between children with HB having different COG stage. (D) Kaplan-Meier method showing prognosis in HB children with different miR-206 expression. (E) Univariate Cox analysis demonstrating the correlation of miR-206 expression with different clinicopathological features. HB, Hepatoblastoma. *P < 0.05, ***P < 0.001.

cated low expression, while 3+ to 4+ indicated high expression. The miR-206 level markedly decreased in HB tissues compared with paired adjacent liver tissues (**Figure 5F**). Besides, the Pearson correlation coefficient analysis demonstrated a significantly negative association between miR-206 and KLB expression (**Figure 5G**). FISH staining of miR-206 negatively correlated with the KLB IHC score in HB tissues (**Figure 5H**). Overall, miR-206 targeted KLB directly and negatively modulated its expression.

Decreased miR-206 levels were associated with poor overall survival of patients with HB

The χ^2 tests and Fisher exact tests were used to explore the correlation of miR-206 levels with clinicopathological variables. Decreased miR-206 expression had a correlation with distant metastasis, recurrence, and higher COG stage (**Figure 6A-C** and **Table 2**). Besides, the overall survival was significantly poorer in patients with HB having lower miR-206 expression compared with those with higher miR-206 expression (**Figure 6D**). Further, univariate and multivariate Cox regression models identified the miR-206 level as the independent risk factor for overall survival in children with HB (**Figure 6E**).

KLB activated the PI3K/Akt/mTOR pathway in HB

Several enriched pathways in HB were disclosed using GSVA (**Figure 7A**). Furthermore, KEGG enrichment analysis and GSEA analysis identified mTORC1 signaling as the key down-

stream signaling of KLB in HB (**Figure 7B** and **7C**). WB analysis revealed that the KLB-KD group had markedly decreased expression of p-PI3K, p-Akt, and p-mTOR compared with the control group, whereas the opposite was observed in the KLB-OE group (**Figure 7D**). LY294002, reported as one of PI3K signaling inhibitors, was used in HB cells to suppress PI3K/Akt/mTOR signaling, which could also be inhibited to a large extent by KLB knockdown (**Figure 7E**). Correspondingly, KLB overexpression rescued the inhibition of LY294002 in HB cells (**Figure 7F**). Besides, IHC analysis in HB tissues from patients indicated a positive correlation between KLB staining and the staining of p-Akt, p-PI3K, or p-mTOR (**Figure 7G-I**). Overall, the results revealed PI3K/Akt/mTOR signaling activated by KLB in HB.

Upregulation of miR-206 inhibited the proliferative, migratory, and invasive capacities of HB cells through targeting KLB

Next, miRNA NC, miR-206 mimic, or miR-206 mimic plus KLB plasmid was transfected into HB cell lines. WB analysis indicated that miR-206 markedly inhibited KLB expression in HB cell lines. KLB overexpression partially rescued the suppressed expression of miR-206 in HB cells (**Figure 8A**). CCK-8, Ki67 IF, and colony formation assay indicated that miR-206 overexpression suppressed the proliferation of HB cells, and this suppression was partially rescued through KLB overexpression (**Figure 8B-D**). Meanwhile, KLB overexpression partially reversed the migratory and invasive capacities of HB cell lines in the presence of miR-206 overexpression (**Figure 8E** and **8F**). The miR-206 mimic was found to suppress the activation of the PI3K/Akt/mTOR pathway, which could be partially rescued through KLB overexpression (**Figure 8G** and **8H**). Taken together, miR-206 inhibited the proliferative, migratory and invasive capacities of HB cell lines through targeting KLB, and the miR-206/KLB axis might be implicated in the PI3K/Akt/mTOR pathway (**Figure 8I**).

Discussion

Over the past decade, the fibroblast growth factor (FGF19)/FGFR4 pathway has achieved adequate attention for its role in the initiation and progression of human tumors [28]. KLB, reported as a co-receptor of FGFR4, exhibited high-affinity interaction with FGF19 in the liver [29]. KLB in association with FGFR4 was suggested to promote apoptosis and inhibit the proliferation of HCC cells [15]. On the contrary, FGF19 overexpression was suggested to suppress sorafenib-induced apoptosis [30]. FGF19 served as an autocrine growth factor for HB cells [31]. In this study, high expression of KLB was observed in HB tissues compared with paired normal liver tissues. In addition, the upregulation of KLB correlated with poor overall survival in pediatric patients with HB. Subsequent experiments further proved that KLB knockdown inhibited the aggressive biological behaviors of HB cells. Therefore, it was hypothesized that KLB might be a molecular switch of the FGF19/FGFR4 pathway in HB. These findings argued in favor of KLB as a potential therapeutic target for pediatric patients with HB. Further studies are warranted for a better understanding of the FGF19/FGFR4/KLB axis in HB. For example, whether the progression of HB could be affected by FGFR4 inhibitors, including FGF401, BLU-554, H3B6527, INCB062079, and so forth, remains a question of interest.

MicroRNAs are short noncoding RNAs that repress gene expression through intermolecular base pairing [18]. The analysis of the GSE75283 dataset revealed that miR-206 levels were markedly reduced in HB tissues compared with normal liver tissues. Subsequent FISH analysis in patients further proved the downregulation of miR-206 in HB tissues compared with control tissues. Clinically, decreased levels of miR-206 correlated with poor prognosis in our patients. In the literature, miR-206 was suggested to be implicated in the pathogenesis of various human tumors other than HB. Specifically, miR-206 could repress the expression of various oncogenes in human tumors, such as epidermal growth factor receptor (EGFR), stanniocalcin 2 (STC2), or cellular mesenchymal to epithelial transition factor (c-Met) in HNSCC [32, 33], cyclin-dependent kinase 9 (CDK9) in HCC [34], and megakaryoblastic leukemia 1 (MKL1)/interleukin 11 (IL11) in breast cancer [25]. The present study demonstrated for the first time that miR-206 overexpression markedly inhibited the proliferative, migratory, and invasive capacities of HB cells, while miR-206 knockdown had an opposite effect. Moreover, the *in vitro* experiment proved

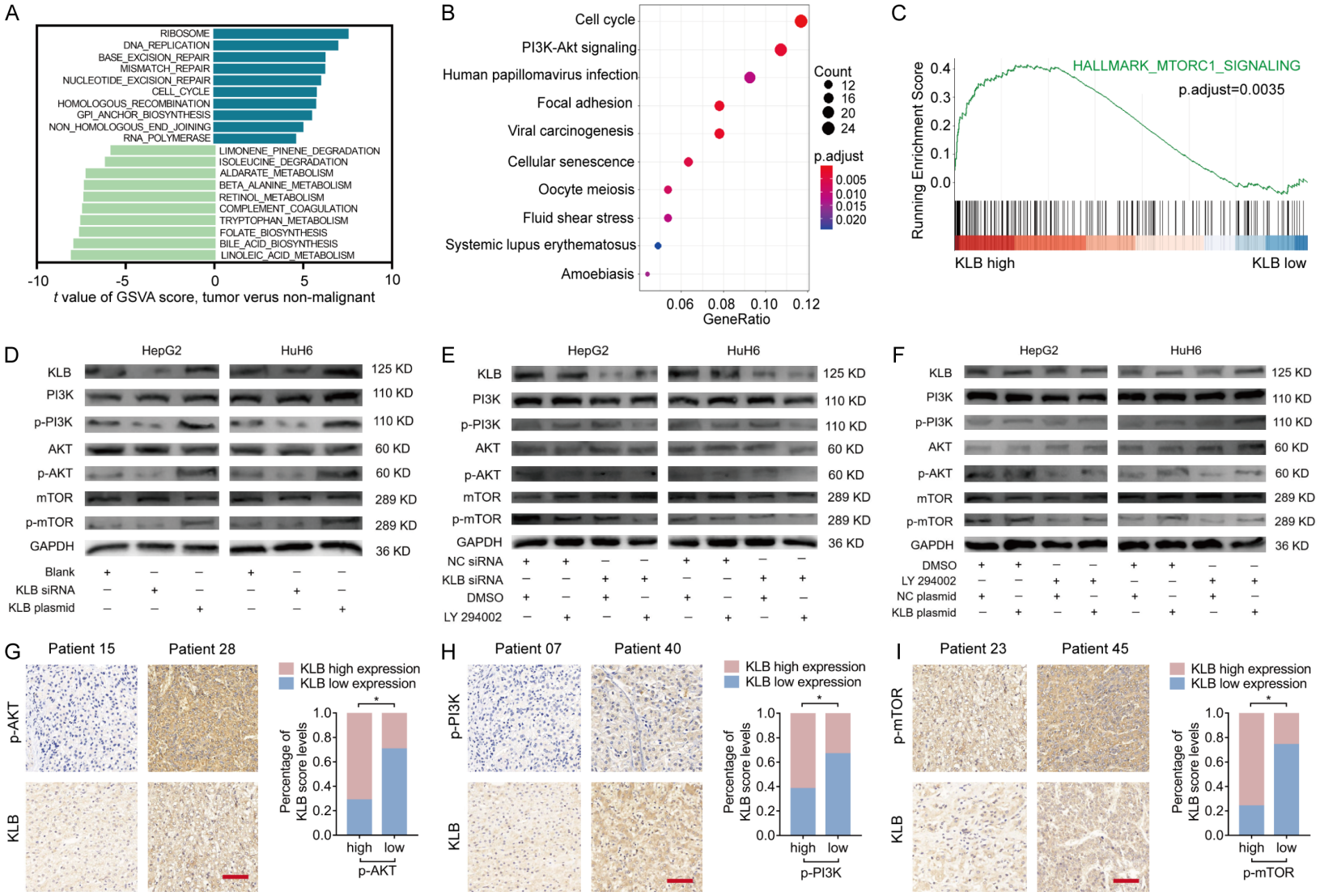

Figure 7. PI3K/Akt/mTOR pathway, critical for HB growth, was inhibited by miR-206. (A) Significantly up- or down-regulated pathways in HB as determined by GSVA. (B) KEGG pathways enrichment analysis (GSE131329 and GSE75271) showing many important pathways in HB. (C) GSEA analysis identifying the mTORC1 pathway as a crucial downstream pathway for KLB. WB analysis showing KLB/PI3K/p-PI3K/AKT/p-Akt/mTOR/p-mTOR expression in HB cell lines after treatment with (D) KLB siRNA, KLB plasmid, or NC; (E) NC siRNA, KLB siRNA, DMSO, or LY294002; (F) LY294002, NC plasmid, DMSO, or KLB plasmid. Representative IHC staining (scale bars, 100 μm) for KLB and (G) p-Akt, (H) p-PI3K, or (I) p-mTOR of HB tissues in patients. GSEA, gene set enrichment analysis; GSVA, gene set variation analysis; HB, Hepatoblastoma; IHC, immunohistochemistry; KEGG, Kyoto Encyclopedia of Genes and Genomes; NC, negative control. *$P < 0.05$. Original WB images are presented in Figures S2 and S3.

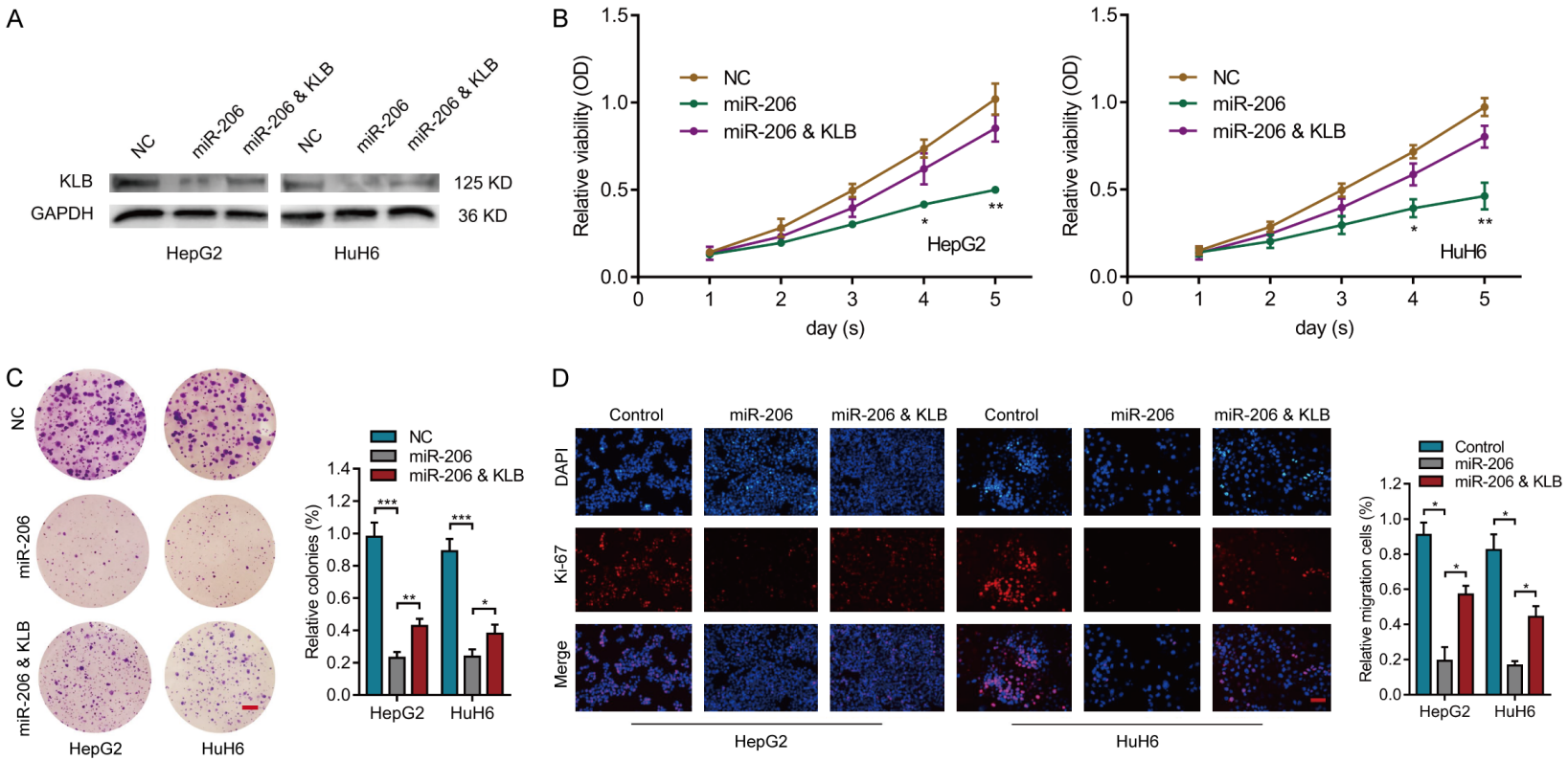
A
NC
miR-206
miR-206 & KLB
NC
miR-206
miR-206 & KLB
KLB
GAPDH
125 KD
36 KD
HepG2
HuH6
B
Relative viability (OD)
NC
miR-206
miR-206 & KLB
day (s)
HepG2
HuH6
C
NC
miR-206
miR-206 & KLB
HepG2
HuH6
Relative colonies (%)
D
Control
miR-206
miR-206 & KLB
DAPI
Ki-67
Merge
Relative migration cells (%)

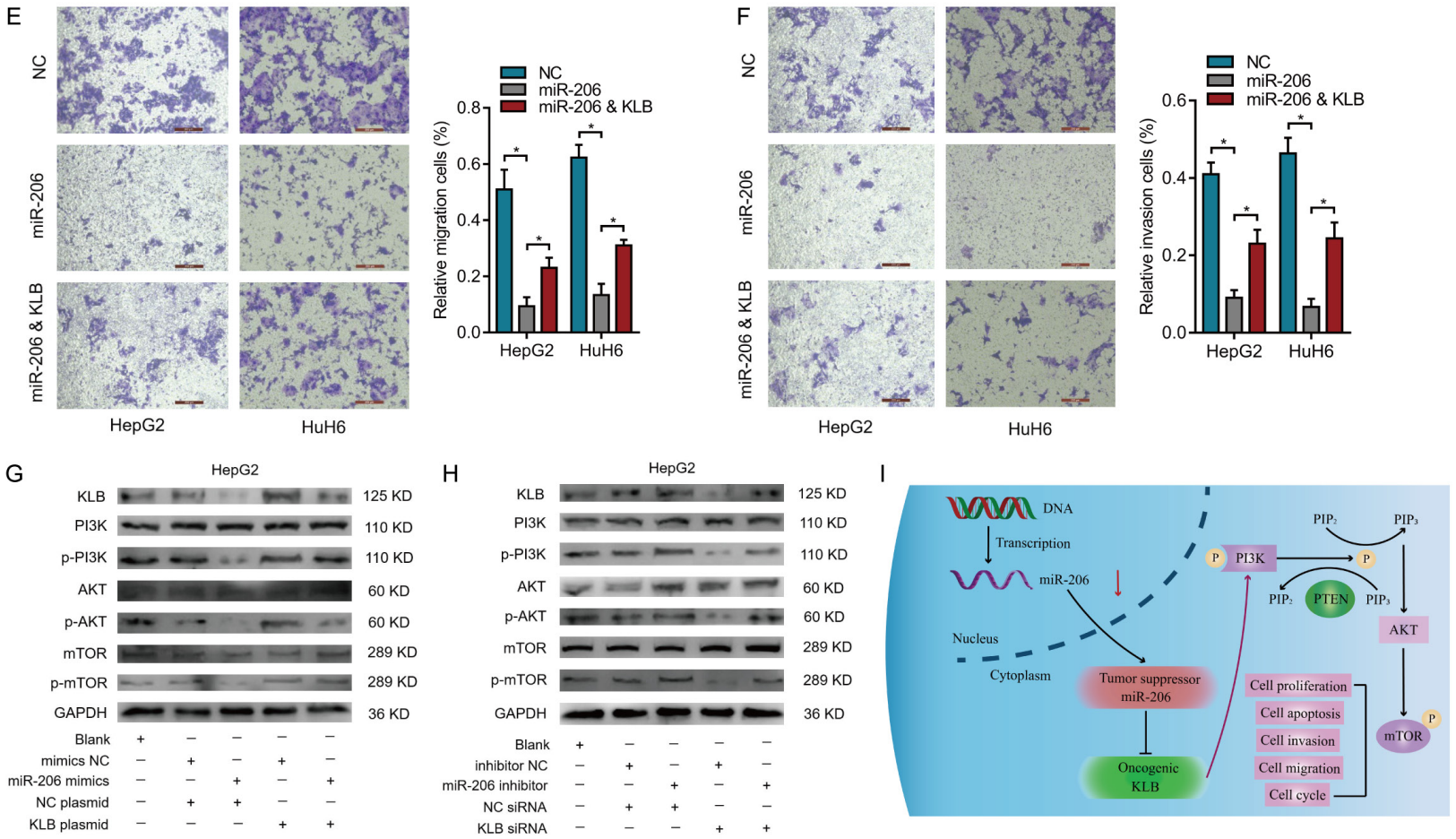

Figure 8. Upregulation of miR-206 inhibited the proliferative and invasive capacities of HB cell lines via targeting KLB. After transfected with NC, miR-206 mimic, or KLB plasmid plus miR-206 mimic in HB cells, (A) WB analysis showing KLB expression among the three groups; (B) CCK-8 assays revealing the proliferation capacity among the three groups; (C) colony formation assays (scale bars, 8 mm) indicating the growth of HB cells among the three groups; (D) IF analysis (scale bars, 100 μm) demonstrating the proliferation ability among different groups as determined by Ki67; Transwell assays (scale bars, 200 μm) revealing (E) the migration capacity, or (F) invasion capacity among the three groups. WB analysis depicting KLB/PI3K/p-PI3K/Akt/p-Akt/mTOR/p-mTOR expression in HepG2 (G) after transfection with NC, miR-206 mimic, or KLB plasmid; (H) after treatment with NC, miR-206 inhibitor, or KLB siRNA. (I) Diagram of the hypothetical mechanism clarifying the effects of miR-206/KLB axis on HB growth by augmenting the PI3K/Akt/mTOR pathway. CCK-8, Cell Counting Kit-8; HB, Hepatoblastoma; IF, immunofluorescence; IHC, immunohistochemistry; NC, negative control; WB, Western blot. *P < 0.05, **P < 0.01, ***P < 0.001. Original WB images are presented in Figure S3.

that KLB overexpression could partially rescue the inhibitory effect of miR-206 overexpression on HB progression.

The PI3K/Akt and the mTOR pathways are both crucial to a wide range of physiological or pathological cellular processes. These two pathways are so closely associated that they can be considered as a single one. The PI3K/Akt/mTOR signaling serves as one of the most frequently hyperactivated signaling cascades in human tumors, including embryonal tumors [35-37]. Additive anti-tumor effects in HB cells were detected after combination chemotherapy with PI3K inhibitors [38]. In tumor cells, p-Akt could inhibit apoptosis [39], and the expression of FGF19/FGFR4 was significantly and positively associated with p-Akt expression [40]. The upregulation of the FGF19/FGFR4/KLB axis contributed to the activation of the PI3K/Akt pathway indirectly in HCC [41]. Correspondingly, KLB knockdown inhibited the proliferative ability of HCC cells by suppressing the phosphorylation of FGF receptor substrate-2α (FRS2α), extracellular signal-regulated kinase (ERK) and Akt [14]. This study found that KLB knockdown promoted apoptosis and suppressed the proliferative, migratory, and invasive capacities of HB cells through inhibiting PI3K/Akt/mTOR signaling. Previous studies reported that rapamycin, a specific mTOR inhibitor, could suppress the proliferative ability of human neuroblastoma cells [42], and enhance the effects of cytotoxic chemotherapy drugs in medulloblastoma cells [43]. This was probably because mTOR inhibitors impeded cells from entering the S-phase from the G1 phase, ultimately leading to apoptosis [37]. The data showed that KLB knockdown enhanced the suppressive influence of LY294002 (a PI3K signaling inhibitor) in HB cells. It was speculated that the suppression of PI3K/Akt/mTOR signaling in combination with other chemotherapeutic drugs, might represent a potential synergistic therapeutic strategy for patients with HB in the future. FGF19 can activate mTORC1 through the Ras-like (Ral) protein in various human tumors [44-47]. In the context of HCC, the FGF19/FGFR4 axis was reported to induce mTORC1 and ERK pathways to converge on S6, and FGF19-induced cell growth and proliferation were abolished after the inhibition of mTORC1 [47]. Besides, FGFR4 upregulation resulted in the phosphorylation of FGFR substrate 2 (FRS2) and recruitment of growth factor receptor-bound protein 2 (GRB2), leading to subsequent activation of mitogen-activated protein kinase (MAPK) and PI3K/Akt signaling pathways involved in cell proliferation and anti-apoptosis [48, 49]. It thus seems reasonable to assume that KLB may regulate PI3K/Akt/mTOR signaling via the FGF19/FGFR4 axis and their downstream signaling. Future studies are needed to validate this hypothesis and provide additional mechanistic insights. In addition, the results also provided ample evidence that miR-206 participated in HB growth through augmenting the PI3K/Akt/mTOR pathway (**Figure 8**). Similarly, previous studies revealed the relationship between miR-206 and the PI3K/Akt/mTOR pathway in other human tumors. For instance, miR-206 suppressed the proliferative and migratory capacities of epithelial ovarian cancer cells through targeting c-Met and inhibiting the Akt/mTOR pathway [50]. Regarding endometrial cancer, miR-206 promoted tumor growth by targeting HDAC and augmenting the PTEN/Akt/mTOR pathway [51].

In conclusion, this study demonstrated that miR-206 negatively regulated KLB expression levels via the PI3K/Akt/mTOR pathway in HB. Besides, the miR-206/KLB axis might be treated as a specific and potent therapeutic target for pediatric patients with HB.

Acknowledgements

The authors are grateful to all members from Department of General Surgery, Shanghai Children's Hospital, Shanghai Jiao Tong University. The present study was funded by National Natural Science Foundation of China (81871194).

Disclosure of conflict of interest

None.

Address correspondence to: Zhibao Lv, Department of General Surgery, Shanghai Children's Hospital, Shanghai Jiao Tong University, No. 24, Lane 1400, West Beijing Road, Shanghai 200040, P. R. China. E-mail: zhibaolyu@sina.cn

References

[1] Tulla M, Berthold F, Graf N, Rutkowski S, von Schweinitz D, Spix C and Kaatsch P. Incidence,

trends, and survival of children with embryonal tumors. Pediatrics 2015; 136: e623-632.
[2] Linabery A and Ross J. Trends in childhood cancer incidence in the U.S. (1992-2004). Cancer 2008; 112: 416-432.
[3] Maibach R, Roebuck D, Brugieres L, Capra M, Brock P, Dall'Igna P, Otte J, De Camargo B, Zsiros J, Zimmermann A, Aronson D, Childs M, Scopinaro M, Morland B, Plaschkes J, Czauderna P and Perilongo G. Prognostic stratification for children with hepatoblastoma: the SIOPEL experience. Eur J Cancer 2012; 48: 1543-1549.
[4] Robinson MD and Oshlack A. A scaling normalization method for differential expression analysis of RNA-seq data. Genome Biol 2010; 11: 1-9.
[5] Sahu A, Mamiya H, Shinde S, Cheikhi A, Winter L, Vo N, Stolz D, Roginskaya V, Tang WY and Croix CS. Age-related declines in α-Klotho drive progenitor cell mitochondrial dysfunction and impaired muscle regeneration. Nat Commun 2018; 9: 1-14.
[6] Razzaque MS. The role of Klotho in energy metabolism. Nat Rev Endocrinol 2012; 8: 579-587.
[7] Lee S, Choi J, Mohanty J, Sousa LP, Tome F, Pardon E, Steyaert J, Lemmon MA, Lax I and Schlessinger J. Structures of β-klotho reveal a 'zip code'-like mechanism for endocrine FGF signalling. Nature 2018; 553: 501-505.
[8] Ito S, Kinoshita S, Shiraishi N, Nakagawa S, Sekine S, Fujimori T and Nabeshima YI. Molecular cloning and expression analyses of mouse βklotho, which encodes a novel Klotho family protein. Mech Dev 2000; 98: 115-119.
[9] Liu Z, Zhang H, Ding S, Qi S, Liu S, Sun D, Dong W, Yin L, Li M and Zhao X. βKlotho inhibits androgen/androgen receptor-associated epithelial-mesenchymal transition in prostate cancer through inactivation of ERK1/2 signaling. Oncol Rep 2018; 40: 217-225.
[10] Liu Z, Qi S, Zhao X, Li M, Ding S, Lu J and Zhang H. Metformin inhibits 17β-estradiol-induced epithelial-to-mesenchymal transition via βKlotho-related ERK1/2 signaling and AMPKα signaling in endometrial adenocarcinoma cells. Oncotarget 2016; 7: 21315.
[11] Li F, Li X, Li Z, Ji W, Lu S and Xia W. βKlotho is identified as a target for theranostics in non-small cell lung cancer. Theranostics 2019; 9: 7474.
[12] Hori S, Miyake M, Onishi S, Tatsumi Y, Morizawa Y, Nakai Y, Anai S, Tanaka N and Fujimoto K. Clinical significance of α- and β-Klotho in urothelial carcinoma of the bladder. Oncol Rep 2016; 36: 2117-2125.
[13] Lin ZZ, Hsu C, Jeng YM, Hu FC, Pan HW, Wu YM, Hsu HC and Cheng AL. Klotho-beta and fibroblast growth factor 19 expression correlates with early recurrence of resectable hepatocellular carcinoma. Liver Int 2019; 39: 1682-1691.
[14] Poh W, Wong W, Ong H, Aung MO, Lim SG, Chua BT and Ho HK. Klotho-beta overexpression as a novel target for suppressing proliferation and fibroblast growth factor receptor-4 signaling in hepatocellular carcinoma. Mol Cancer 2012; 11: 1-10.
[15] Luo Y, Yang C, Lu W, Xie R, Jin C, Huang P, Wang F and McKeehan WL. Metabolic regulator βKlotho interacts with fibroblast growth factor receptor 4 (FGFR4) to induce apoptosis and inhibit tumor cell proliferation. J Biol Chem 2010; 285: 30069-30078.
[16] Dongiovanni P, Crudele A, Panera N, Romito I, Meroni M, De Stefanis C, Palma A, Comparcola D, Fracanzani A, Miele L, Valenti L, Nobili V and Alisi A. β-Klotho gene variation is associated with liver damage in children with NAFLD. J Hepatol 2020; 72: 411-419.
[17] Lee K, Jang Y, Cha S, Kim M, Park K, Eom Y and Baik S. Expression of fibroblast growth factor 21 and β-klotho regulates hepatic fibrosis through the nuclear factor-κB and c-Jun N-terminal kinase pathways. Gut Liver 2018; 12: 449-456.
[18] Gebert LF and MacRae IJ. Regulation of microRNA function in animals. Nat Rev Mol Cell Biol 2019; 20: 21-37.
[19] von Frowein J, Hauck SM, Kappler R, Pagel P, Fleischmann KK, Magg T, Cairo S, Roscher A, von Schweinitz D and Schmid I. MiR-492 regulates metastatic properties of hepatoblastoma via CD44. Liver Int 2018; 38: 1280-1291.
[20] von Frowein J, Pagel P, Kappler R, von Schweinitz D, Roscher A and Schmid I. MicroRNA-492 is processed from the keratin 19 gene and up-regulated in metastatic hepatoblastoma. Hepatology 2011; 53: 833-842.
[21] Cristóbal I, Sanz-Álvarez M, Luque M, Caramés C, Rojo F and García-Foncillas J. The role of MicroRNAs in hepatoblastoma tumors. Cancers (Basel) 2019; 11: 409.
[22] Taulli R, Bersani F, Foglizzo V, Linari A, Vigna E, Ladanyi M, Tuschl T and Ponzetto C. The muscle-specific microRNA miR-206 blocks human rhabdomyosarcoma growth in xenotransplanted mice by promoting myogenic differentiation. J Clin Invest 2009; 119: 2366-2378.
[23] Zhang H, Wang J, Ren T, Huang Y, Liang X, Yu Y, Wang W, Niu J and Guo W. Bone marrow mesenchymal stem cell-derived exosomal miR-206 inhibits osteosarcoma progression by targeting TRA2B. Cancer Lett 2020; 490: 54-65.
[24] Singh A, Happel C, Manna SK, Acquaah-Mensah G, Carrerero J, Kumar S, Nasipuri P, Krausz KW, Wakabayashi N and Dewi R. Transcription

factor NRF2 regulates miR-1 and miR-206 to drive tumorigenesis. J Clin Invest 2013; 123: 2921-2934.
[25] Samaeekia R, Adorno-Cruz V, Bockhorn J, Chang YF, Huang S, Prat A, Ha N, Kibria G, Huo D and Zheng H. miR-206 inhibits stemness and metastasis of breast cancer by targeting MKL1/IL11 pathway. Clin Cancer Res 2017; 23: 1091-1103.
[26] Zhang H, Li M, Zheng X, Sun Y, Wen Z and Zhao X. Endometriotic stromal cells lose the ability to regulate cell-survival signaling in endometrial epithelial cells in vitro. Mol Hum Reprod 2009; 15: 653-663.
[27] Cui XC, Wang ZF, Liu LW, Liu X, Zhang DD, Li JH, Zhu JM, Pan JT, Zhang D and Cui GY. The long non-coding RNA ZFAS1 sponges miR-193a-3p to modulate hepatoblastoma growth by targeting RALY via HGF/c-Met pathway. Front Cell Dev Biol 2019; 7: 271.
[28] Wu X, Ge H, Lemon B, Vonderfecht S, Weiszmann J, Hecht R, Gupte J, Hager T, Wang Z and Lindberg R. FGF19-induced hepatocyte proliferation is mediated through FGFR4 activation. J Biol Chem 2010; 285: 5165-5170.
[29] Lin BC, Wang M, Blackmore C and Desnoyers LR. Liver-specific activities of FGF19 require Klotho beta. J Biol Chem 2007; 282: 27277-27284.
[30] Gao L, Wang X, Tang Y, Huang S, Hu CA and Teng Y. FGF19/FGFR4 signaling contributes to the resistance of hepatocellular carcinoma to sorafenib. J Exp Clin Cancer Res 2017; 36: 1-10.
[31] Elzi DJ, Song M, Blackman B, Weintraub ST, López-Terrada D, Chen Y, Tomlinson GE and Shiio Y. FGF19 functions as autocrine growth factor for hepatoblastoma. Genes Cancer 2016; 7: 125.
[32] Koshizuka K, Hanazawa T, Fukumoto I, Kikkawa N, Matsushita R, Mataki H, Mizuno K, Okamoto Y and Seki N. Dual-receptor (EGFR and c-MET) inhibition by tumor-suppressive miR-1 and miR-206 in head and neck squamous cell carcinoma. J Hum Genet 2017; 62: 113-121.
[33] Li T, Qin Y, Zhen Z, Shen H, Cong T, Schiferle E and Xiao S. Long non-coding RNA HOTAIR/microRNA-206 sponge regulates STC2 and further influences cell biological functions in head and neck squamous cell carcinoma. Cell Prolif 2019; 52: e12651.
[34] Pang C, Huang G, Luo K, Dong Y, He F, Du G, Xiao M and Cai W. miR-206 inhibits the growth of hepatocellular carcinoma cells via targeting CDK9. Cancer Med 2017; 6: 2398-2409.
[35] Zhang J, Hu S, Schofield DE, Sorensen PH and Triche TJ. Selective usage of D-Type cyclins by Ewing's tumors and rhabdomyosarcomas. Cancer Res 2004; 64: 6026-6034.
[36] Hartmann W, Digon-Söntgerath B, Koch A, Waha A, Endl E, Dani I, Denkhaus D, Goodyer CG, Sörensen N and Wiestler OD. Phosphatidylinositol 3'-kinase/AKT signaling is activated in medulloblastoma cell proliferation and is associated with reduced expression of PTEN. Clin Cancer Res 2006; 12: 3019-3027.
[37] Vivanco I and Sawyers CL. The phosphatidylinositol 3-Kinase AKT pathway in human cancer. Nat Rev Cancer 2002; 2: 489-501.
[38] Hartmann W, Küchler J, Koch A, Friedrichs N, Waha A, Endl E, Czerwitzki J, Metzger D, Steiner S and Wurst P. Activation of phosphatidylinositol-3'-kinase/AKT signaling is essential in hepatoblastoma survival. Clin Cancer Res 2009; 15: 4538-4545.
[39] Franke T, Kaplan D and Cantley L. PI3K: downstream AKTion blocks apoptosis. Cell 1997; 88: 435-437.
[40] Jaakkola S, Salmikangas P, Nylund S, Partanen J, Armstrong E, Pyrhönen S, Lehtovirta P and Nevanlinna H. Amplification of fgfr4 gene in human breast and gynecological cancers. Int J Cancer 1993; 54: 378-382.
[41] Subbiah V and Pal S. Precision oncology for hepatocellular cancer: slivering the liver by FGF19-FGF4-KLB pathway inhibition. Cancer Discov 2019; 9: 1646-1649.
[42] Mondesire W, Jian W, Zhang H, Ensor J, Hung M, Mills G and Meric-Bernstam F. Targeting mammalian target of rapamycin synergistically enhances chemotherapy-induced cytotoxicity in breast cancer cells. Clin Cancer Res 2004; 10: 7031-7042.
[43] Geoerger B, Kerr K, Tang C, Fung K, Powell B, Sutton L, Phillips P and Janss A. Antitumor activity of the rapamycin analog CCI-779 in human primitive neuroectodermal tumor/medulloblastoma models as single agent and in combination chemotherapy. Cancer Res 2001; 61: 1527-1532.
[44] Oxford G, Owens CR, Titus BJ, Foreman TL, Herlevsen MC, Smith SC and Theodorescu D. RalA and RalB: antagonistic relatives in cancer cell migration. Cancer Res 2005; 65: 7111-7120.
[45] Bodemann BO and White MA. Ral GTPases and cancer: linchpin support of the tumorigenic platform. Nat Rev Cancer 2008; 8: 133-140.
[46] Gao L, Lang L, Zhao X, Shay C, Shull AY and Teng Y. FGF19 amplification reveals an oncogenic dependency upon autocrine FGF19/FGFR4 signaling in head and neck squamous cell carcinoma. Oncogene 2018; 38: 2394-2404.
[47] Wan ZY, Tian JS, Tan HW, Chow AL, Sim AY, Ban KH and Long YC. Mechanistic target of rapamycin complex 1 is an essential mediator of metabolic and mitogenic effects of fibroblast growth factor 19 in hepatoma cells. Hepatology 2016; 64: 1289-1301.
[48] Katoh M and Nakagama H. FGF receptors: cancer biology and therapeutics. Med Res Rev 2014; 34: 280-300.

[49] Touat M, Ileana E, Postel-Vinay S, André F and Soria JC. Targeting FGFR signaling in cancer. Clin Cancer Res 2015; 21: 2684-2694.

[50] Dai C, Xie Y, Zhuang X and Yuan Z. MiR-206 inhibits epithelial ovarian cancer cells growth and invasion via blocking c-Met/AKT/mTOR signaling pathway. Biomed Pharmacother 2018; 104: 763-770.

[51] Zheng Y, Yang X, Wang C, Zhang S, Wang Z, Li M, Wang Y, Wang X and Yang X. HDAC6, modulated by miR-206, promotes endometrial cancer progression through the PTEN/AKT/mTOR pathway. Sci Rep 2020; 10: 3576.

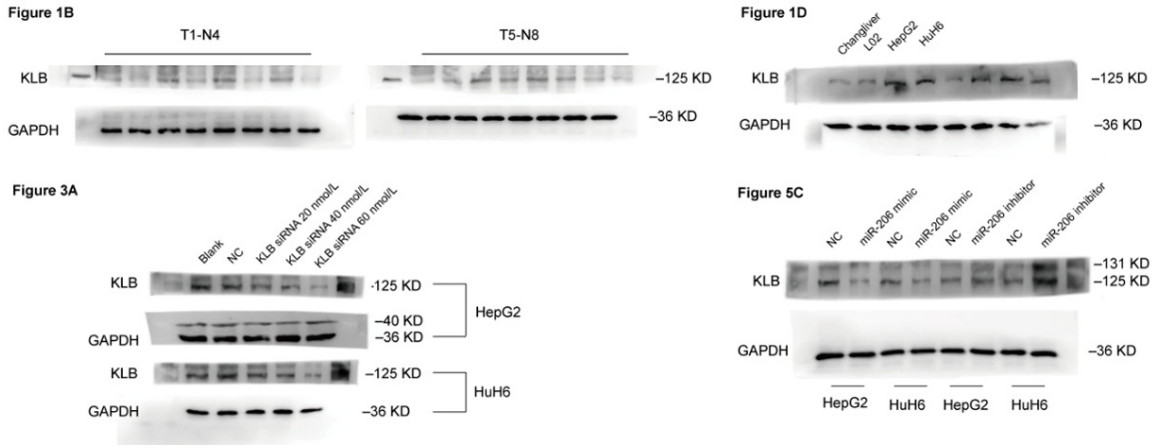

Figure S1. Original Western blot images of **Figures 1B**, **1D**, **3A** and **5C**.

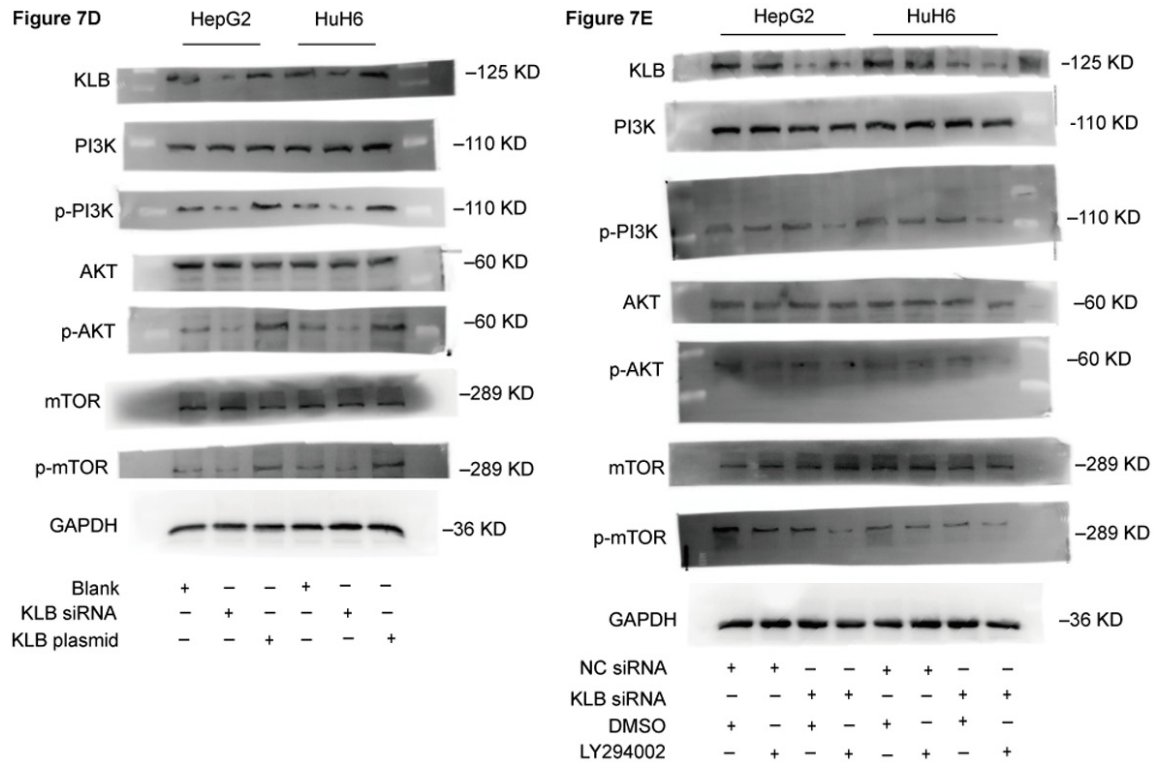

Figure S2. Original Western blot images of **Figure 7D** and **7E**.

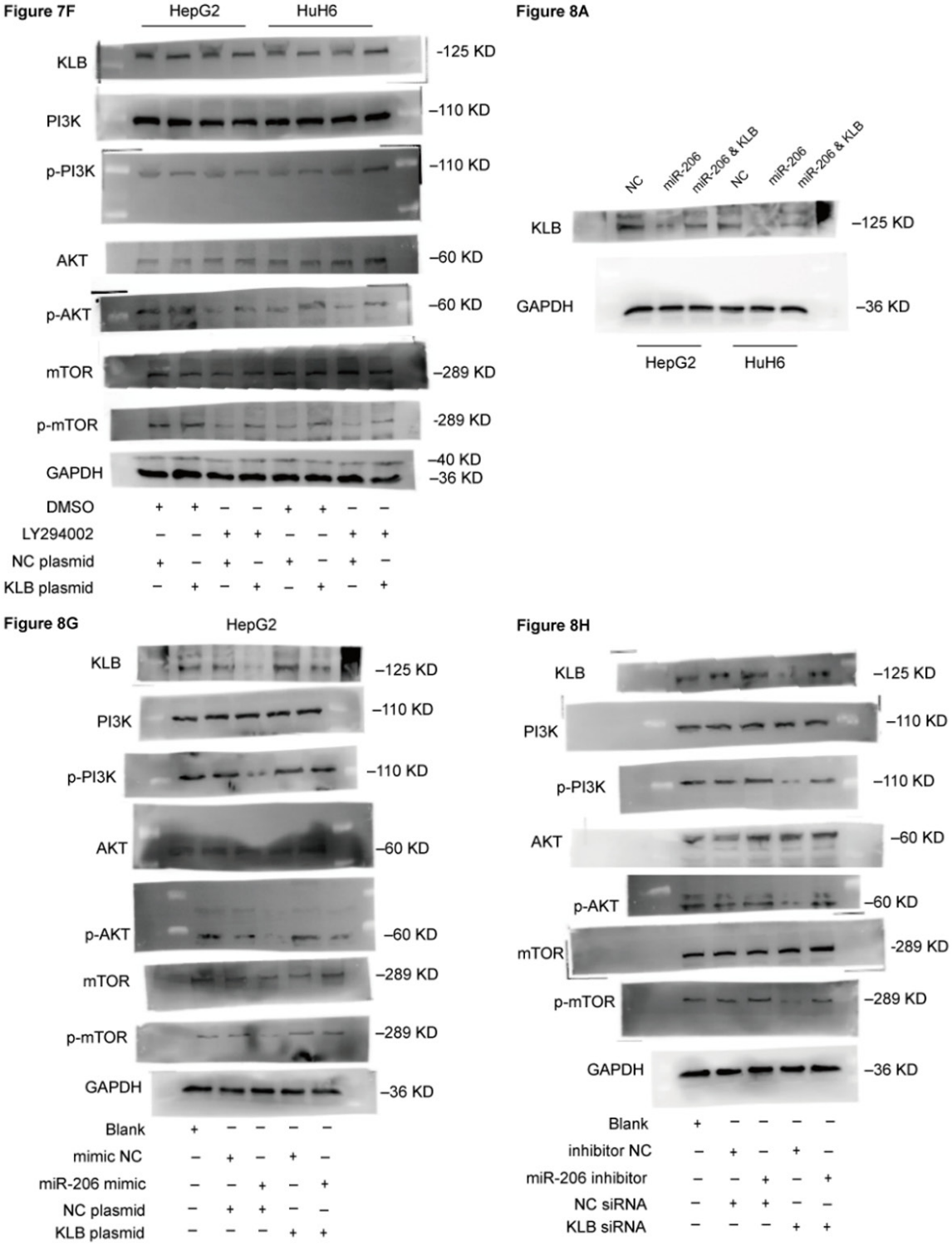

Figure S3. Original Western blot images of **Figures 7F**, **8A**, **8G** and **8H**.